Characterization of Composites for Use in the Ball-Joints of the Maeslant Storm Surge Barrier

W. Van Paepegem,[1] J. Degrieck,[1] P. Samyn,[1] P. De Baets,[1] L. Van Schepdael,[2] J.S. Leendertz[3]
[1]*Department of Mechanical Construction and Production, Ghent University, 9000 Gent, Belgium*

[2]*SOLICO BV, Solutions in Composites, The Netherlands*

[3]*Ministry of Transport, Public Works and Water Management, The Netherlands*

In 2004, the rehabilitation works of the Maeslant storm surge barrier in the Netherlands were finished. The two gates of the barrier are attached to a pivotal point on both banks. The pivotal points are designed as two large ball-joints (10 m diameter) that must allow for both horizontal and vertical movements of the gates. Five hundred individual composite material discs provide a low friction sliding contact with the ball. Two designs for the composite material discs are discussed in this article: (i) a polyester/polyester disc with a Teflon coating and (ii) an UHMWPE (ultra-high molecular weight polyethylene) disc with a reinforcing carbon/epoxy ring. The test methods for characterization of the composite materials are presented. It is shown that internationally standardized test methods do not provide all necessary information and that additional measurements have to be made. Based on the results of these tests, the best design has been integrated in the storm surge barrier. POLYM. COMPOS., 28:470–478, 2007. © 2007 Society of Plastics Engineers

INTRODUCTION

The south-west part of the Netherlands is located in a low-lying delta, where the Rhine and IJssel rivers run into the North Sea. In 1953, the fatal combination of a north-western storm and spring tide resulted in the inundation of large parts of the provinces of Zeeland and South Holland. To prevent a repetition of the disaster, a set of measures were laid down in the Delta Act. Large primary dams were constructed and dikes were elevated. As the seaports of Rotterdam and Antwerp had to remain accessible, no dams could be built in the New Waterway and the Western Scheldt. The elevation of the dikes was not an option as well. Finally, in the 1980s, a movable storm surge barrier appeared to be the most attractive in terms of cost, environmental effects, and safety [1].

This Maeslant storm surge barrier consists of two hollow semicircular gates attached by means of steel arms to a pivotal point on both banks, as illustrated in Fig. 1. In the event of a storm tide, the "parking" docks are filled with water, so that the hollow gates start to float and can be turned into the New Waterway. Once the gates meet, the cavities are filled with water and the gates sink to the bottom, thus sealing off the 360 m wide opening.

The two ball-joints are designed to ensure that the gates can move in all directions, both horizontally (when the gates are turned into the waterway) and vertically (upon submersion). With a diameter of 10 m and a weight of 680 tons, the ball-joints are more than three times as big as the largest ball-joint ever used. In the front, rear and bottom pedestals of the ball-joints, 500 machined holes provide place for the composite material discs that must guarantee low friction sliding contacts at high normal pressures (up to 150 MPa), as illustrated in Fig. 2.

In this article, the qualification tests for the composite material discs are discussed. Two different material systems have been tested: (i) a polyester/polyester disc with a Teflon coating and (ii) an UHMWPE (ultra-high molecular weight polyethylene) disc with a reinforcing carbon/epoxy ring.

DESIGN SPECIFICATIONS

When the barrier was commissioned in 1997, the convex and concave surfaces of the ball joint were covered with one layer, a mixture of MoS_2 and polytetra fluorethylene (PTFE), in order to obtain a low static and dynamic design value for friction resistance (≤ 0.15). An additional layer of PTFE had been applied for "run in" purposes, to overcome the damaging effect of the initial friction.

In 1999 after a test closing, wear marks were observed at the bottom concave bearings and the ring elements. These wear marks included loss of MoS_2 at some spots of

Correspondence to: Wim Van Paepegem; e-mail: Wim.VanPaepegem@UGent.be
Contract grant sponsor: Fund for Scientific Research–Flanders (FWO).
DOI 10.1002/pc.20306
Published online in Wiley InterScience (www.interscience.wiley.com).

FIG. 1. View on the Maeslant storm surge barrier [1]. [Color figure can be viewed in the online issue, which is available at www.interscience.wiley.com.]

the ball at the north abutment and cold welding between the convex and the concave bearings at the south abutment. In the following years, similar damage was observed.

The wear did not threaten immediately the functionality of the barrier, but it caused large repair works including an "out-of-service" period. Further, it was difficult to achieve the exact geometry, which would cause an increasing need for repair in the future. This was unacceptable for the owner, *Rijkswaterstaat Directie Zuid Holland* that initiated a project for improvement of the ball bearing.

The design specifications for the re-design of the ball-joint surfaces are summarized in Table 1 [2].

In a preliminary phase, three options were selected for both the convex and concave surfaces:

- convex surface: bare cast steel, a metal spray coating or paint,
- concave surface: UHMWPE and two types of polyester/polyester discs with Teflon coating

For the convex surfaces, the bare cast steel would show too much corrosion and metal spray coatings would need much development before they could have been applied on site, so a paint (Hempaquick Alkyd primer) was selected as the most favorable solution.

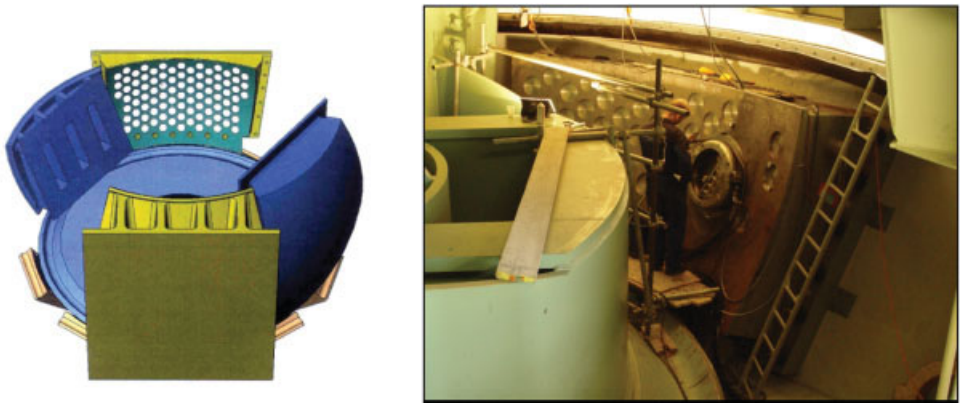

FIG. 2. Top view of the ball-joint (left) and machining of the 500 holes in the pedestals (right). [Color figure can be viewed in the online issue, which is available at www.interscience.wiley.com.]

TABLE 1. Design specifications for the redesign of the ball joint surfaces [2].

	Aspect	Requirement
1.	Global behavior	modification of the space of 20 mm between the radius of the convex parts and the concave parts shall not affect substantially the resultants and their positions
2.	Resistance of the steel structures	the existing resistance of the steel structures of the trusses and the steel structure of the ball joint shall not be exceeded
3.	Friction coefficient	shall not exceed 0.25
4.	Clearance	sufficient for the convex rear bearing to pass the concave rear bearing during floating out
5.	Wear	total wear path of 300 m over 5 years, being the slide path for the worst location
6.	Postcritical behavior	the deformation due to elastic and plastic compression and the loss of material due to wear shall not lead to contact between the convex and the concave parts
7.	Durability	the minimum requirement is related to the functioning over 1 year
8.	Environment	the materials shall not be in conflict with the environmental laws
9.	Manufacturing and erection	the requirements are derived from the design
10.	Maintenance	the minimum requirements relate to a period of 1 year
11.	Research and development	no fundamental research, only further development of known materials and techniques

For the concave surfaces, UHMWPE and the polyester/polyester discs with Teflon coating were selected and comparative tests were performed.

POLYESTER/POLYESTER DISC WITH TEFLON COATING

Figure 3 shows the polyester/polyester disc with Teflon coating. The composite sliding pads consist of woven polyester fabrics (90°) impregnated with a thermosetting polyester resin. For use in the ball-joints, the elastic properties and the behavior beyond the elastic region had to be characterized. In-service deformations of 10% and more could be expected.

The large thickness of the discs and the need for determination of all independent elastic properties of the orthotropic material lead to the design of nonstandard testing conditions. Eight elastic properties had to be determined: E_{11}, E_{22}, E_{33}, G_{13}, G_{23}, ν_{12}, ν_{23}, and ν_{31}. The identification of the shear modulus G_{12} could be excluded because of the axisymmetric loading conditions. Four types of tests were performed: (i) uniaxial tensile tests, (ii) uniaxial compression tests, (iii) short-beam three-point bending tests, and (iv) creep tests.

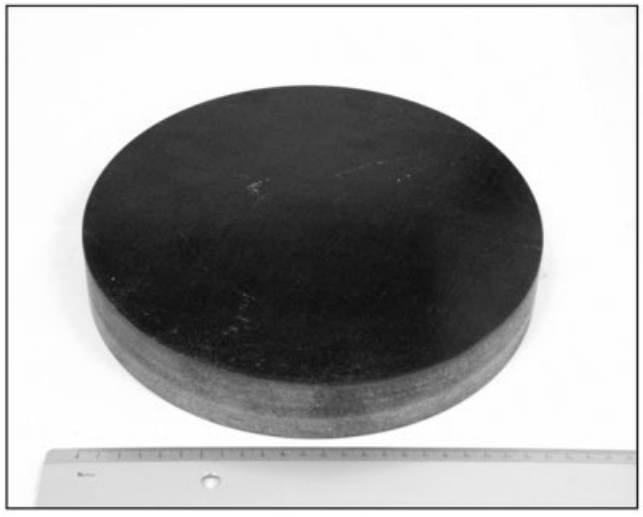

FIG. 3. View of the polyester/polyester disc with Teflon coating.

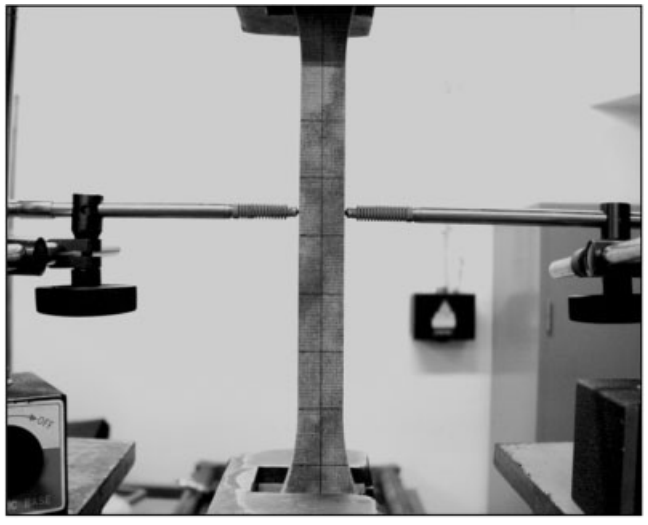

FIG. 4. Experimental set-up for the tensile tests.

Uniaxial Tensile Tests

Figure 4 shows the experimental set-up for the tensile tests. Extensometers, strain gauges, and moiré gratings could not be applied to the specimens, because of the large thickness and the bonding problems onto the surface. Therefore, a geometric grid was drawn onto the specimen's surface. The LVDT's were used to measure the transverse contraction. The specimens were machined into a dogbone shape to guarantee a uniform stress distribution in the midsection of the specimen.

Tensile tests on the 0° stacking sequence yielded the values of E_{11} and ν_{12}. Tensile tests on the 90° stacking sequence were used to measure E_{22} and ν_{23} (by changing the position of the LVDT's). The 45° stacking sequence was used to measure $E_{xx,45°}$ and $\nu_{xy,45°}$.

Figure 5 shows the measured stress–strain curve for the 0° stacking sequence. The open circles indicate the strains calculated from the geometrical grid, while the solid line corresponds with the strains calculated from the machine displacement. As both measurements agree very well, the slip in the grips could be neglected.

Figure 6 shows the fracture patterns for the three stacking sequences. Extensive delaminations were found to occur, already at the early loading stage.

The measured elastic and strength properties are summarized in Table 2.

Uniaxial Compression Tests

Uniaxial compression tests in the thickness direction of the composite material provided the values of E_{33}, ν_{32},

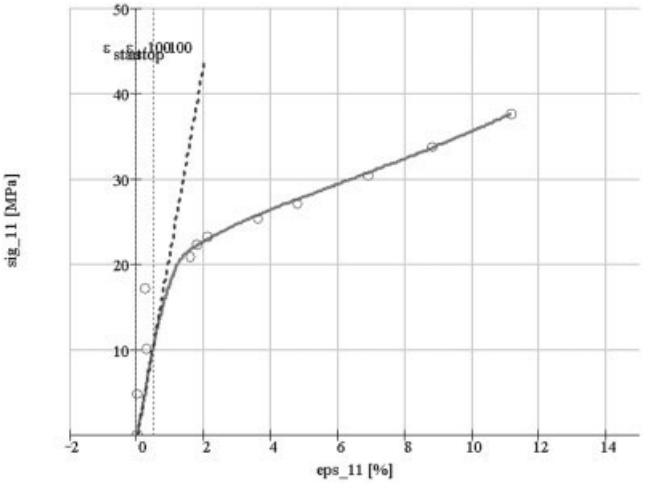

FIG. 5. Stress–strain curve for the 0° stacking sequence.

DOI 10.1002/pc

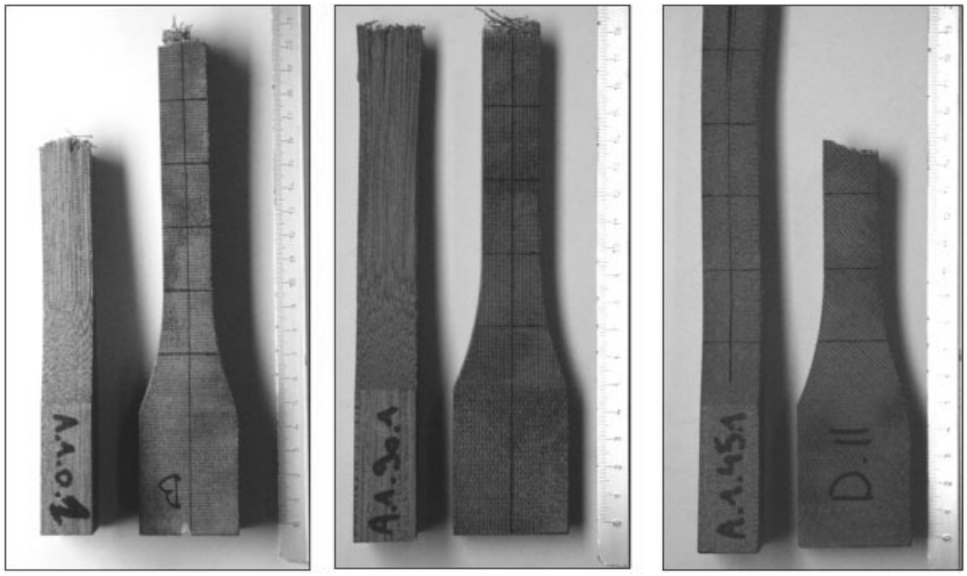

FIG. 6. Fracture patterns of the polyester/polyester composite for the stacking sequences (i) 0 °, (ii) 90°, and (iii) 45°.

and ν_{31}. Figure 7 shows the experimental set-up (left) and the typical shear failure pattern in compression (right).

A typical result is shown in Fig. 8.

The measured elastic and strength properties are listed in Table 3.

TABLE 2. Measured elastic and strength properties by uniaxial tensile tests.

E_{11}	2.36 GPa
E_{22}	2.19 GPa
$E_{xx,45°}$	2.16 GPa
ν_{12}	0.30–0.35
ν_{23}	0.45–0.50
$\nu_{xy,45°}$	0.45–0.50
X_T	49.8 MPa
Y_T	60.4 MPa
$\sigma^{ult}_{xx,45°}$	49.5 MPa
ε^{ult}_{11}	0.175
ε^{ult}_{22}	0.19
$\varepsilon^{ult}_{xx,45°}$	0.336

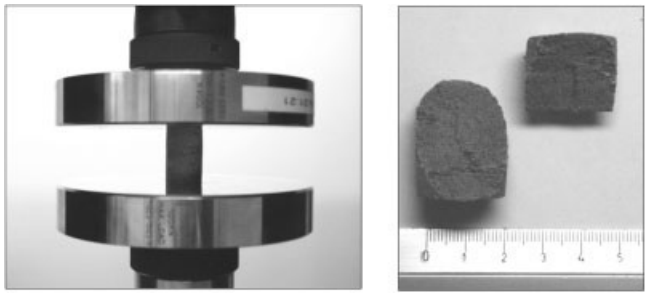

FIG. 7. Compression tests: experimental set-up (left) and failed specimen (right).

Short-Beam Three-Point Bending Tests

No standard test methods were available to obtain the values of G_{13} and G_{23}. Therefore, a combined numerical/experimental approach was chosen. Short-beam three-point bending tests were performed on the 0° and 90° stacking sequence, as shown in Fig. 9.

Numerical optimization of the load-displacement path and the discrete displacement field (measured by the

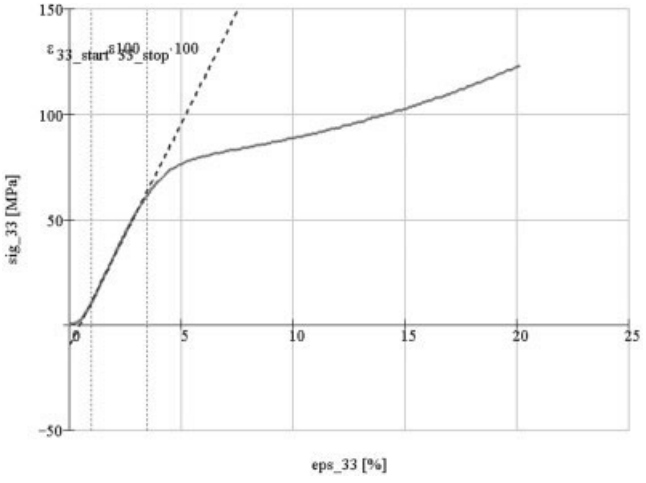

FIG. 8. Compressive stress–strain data.

TABLE 3. Measured elastic and strength properties by compression tests.

E_{33}	2.14 GPa
$\nu_{32} \approx \nu_{31}$	0.2–0.25
Z_C	219 MPa
ε^{ult}_{33}	0.341

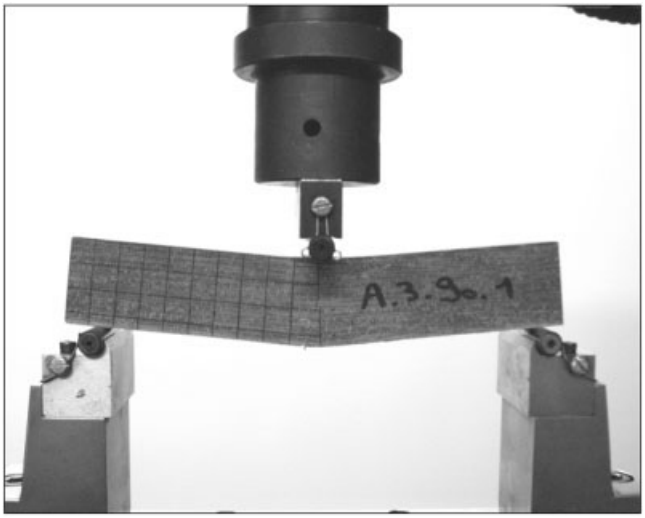

FIG. 9. Short-beam three-point bending tests.

geometric grid) yielded the values of G_{13} and G_{23}. Figure 10 shows the simulated shear strain γ_{13}. The simulated value of 0.6% in the midsection between the support and the load striking edge at a load of 4 kN shows good agreement with the corresponding experimental values for the same load.

Creep Tests

Finally, creep tests were considered where two specimens with Teflon coating were placed side-to-side to obtain symmetrical loading conditions. A schematic set-up is shown in Fig. 11. A constant stress was applied and the increase of axial compressive strain and lateral expansion were measured.

The creep response showed a significant permanent deformation, as well as sliding off of the Teflon coating. Figure 12 shows a pair of tested Teflon-coated specimens and the measured creep strains for one of the specimens.

Additional tests on specimens without the Teflon coating showed the same behavior. Figure 13 shows the specimens after creep tests at (i) 30 MPa, (ii) 60 MPa, (iii) 90 MPa, and (iv) 120 MPa.

In view of the very high pressure loads on the ball-joint and the large permanent deformation of the material, this option was abandoned and another design was put forward.

UHMWPE DISC WITH REINFORCING CARBON/EPOXY RING

In the second design, a disc of ultra-high molecular weight polyethylene (UHMWPE) is locked up by a reinforcing carbon/epoxy ring. The high pressure loads on top of the disc cause the polyethylene to yield. The hydrostatic pressure in the bulk polyethylene results in high hoop stresses in the filament wound carbon/epoxy ring, which is also loaded with high pressure on its top surface.

Figure 14 shows a picture of this UHMWPE disc with reinforcing carbon/epoxy ring.

Figure 15 shows the geometry of the filament wound carbon/epoxy ring (top), the top and bottom part of the

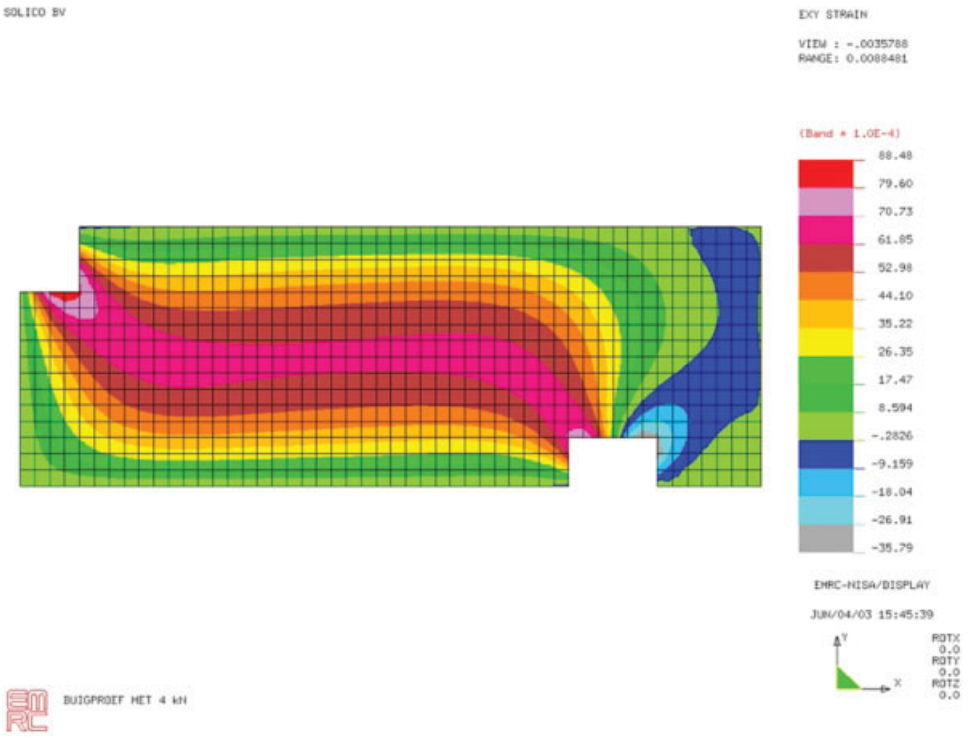

FIG. 10. Finite element simulation of the short-beam three-point bending test (courtesy of SOLICO, solutions in composites). [Color figure can be viewed in the online issue, which is available at www.interscience.wiley.com.]

 DOI 10.1002/pc

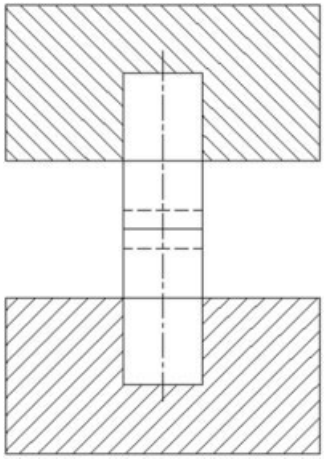

FIG. 11. Testing procedure for the creep tests.

UHMWPE disc (middle), and the assembly of the UHMWPE disc and the carbon/epoxy ring (bottom).

The elastic properties of the constituent materials (polyethylene, carbon fiber, and epoxy matrix) were provided by the suppliers. Some of the properties were checked again. The values are summarized in Table 4.

The main concern in this second design was with the transverse shear strength of the filament wound carbon/epoxy ring. Indeed, the convex surface of the ball-joint makes contact with the surface of the UHMWPE pad. Depending on the position of the UHMWE pad in the pedestals (see Fig. 2), the contact pressure will vary, and as a consequence, the contact area between the convex surface and the individual composite discs as well.

Figure 16 shows a finite element simulation of the contact between the convex surface of the steel ball-joint and the UHMWPE pad with carbon/epoxy ring for two different loading conditions: (i) a normal force of 100 kN and (ii) a normal force of 2,500 kN. The picture shows the calculated stresses through the thickness.

For normal loads above 2,500 kN, the convex surface makes contact with the entire surface of the UHMWPE disc.

The average contact pressure can increase up to values of 163 MPa for the most heavily loaded pads (total normal force of 8,000 kN). As the yield strength of the UHMWPE polymer is only 17 MPa, the polyethylene behaves as a bulk material and the reinforcing carbon/epoxy ring is loaded with radial and transverse compressive stresses. The combination of these loads on the carbon/epoxy ring leads to high transverse shear stresses (up to 80 MPa).

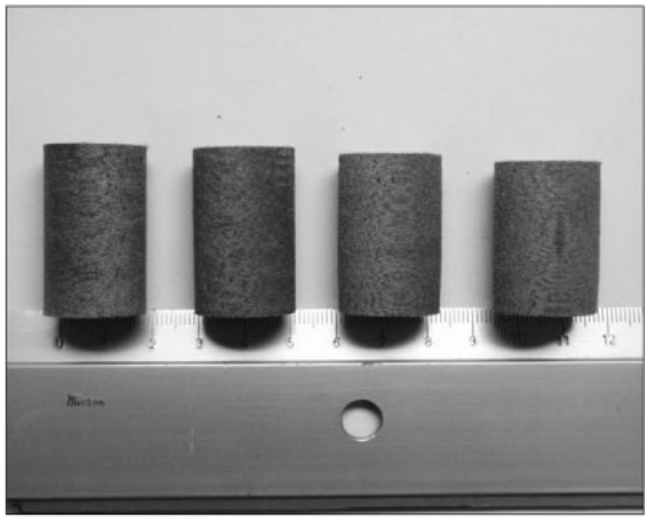

FIG. 13. Specimens after creep tests at (i) 30 MPa, (ii) 60 MPa, (iii) 90 MPa, and (iv) 120 MPa.

As the carbon/epoxy ring was manufactured by unidirectional hoop winding, the shear strength transverse to the fiber was largely attributed to the matrix. To assess this shear strength, three types of qualification tests were designed:

- determination of fiber volume content: too high fiber volume fractions would lead to high concentrations in the fiber/matrix interface region [3] and would result in a poor shear strength transverse to the fiber.
- uniaxial compression tests: through-the-thickness compression tests lead to shear failure transverse to the fiber and are thus a measure for the transverse shear strength.
- short-beam three-point bending tests: these tests prove to

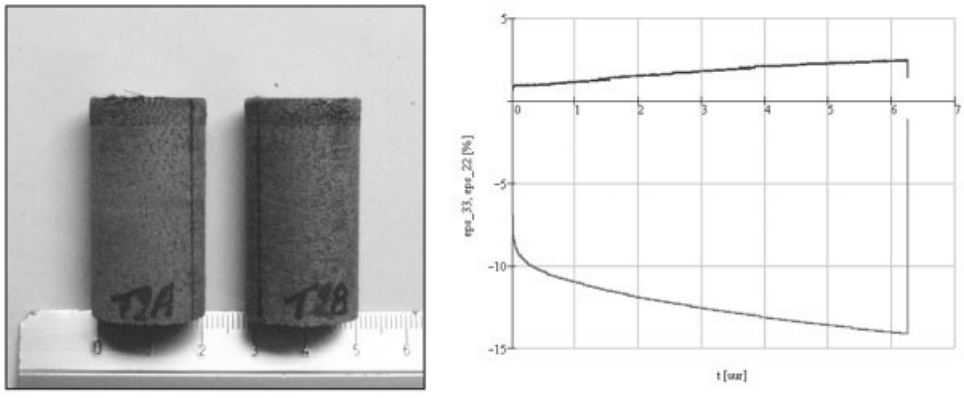

FIG. 12. Pair of teflon-coated specimens after side-to-side creep test at 60 MPa (left) and measured axial compressive strain (ε 33) and lateral expansion (ε 22) (right).

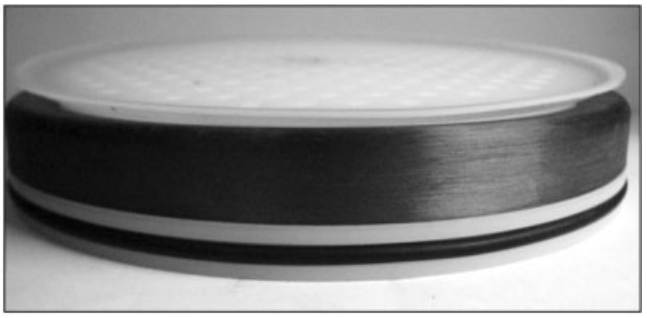

FIG. 14. Picture of the UHMWPE disc with a reinforcing carbon/epoxy ring.

be a reliable indicator of quality and delamination resistance of the composite ring.

Determination of Fiber Volume Content

The fiber volume content was determined by matrix digestion, according to the ASTM standard D3171–99 Standard test methods for constituent content of composite materials. The measured fiber volume content was to stay below 63%.

TABLE 4. Elastic properties of the constituent materials.

UHMWPE	
E	720 MPa
ν	0.45
Carbon/epoxy ring	
E_{11}	150 GPa
$E_{22} = E_{33}$	9 GPa
$\nu_{12} = \nu_{13}$	0.34
ν_{23}	0.5
$G_{12} = G_{13}$	4 GPa
G_{23}	3 GPa

Uniaxial Compression Tests

Uniaxial compression tests were performed on small segments of the ring. Load was applied through the thickness of the ring and a typical shear failure was obtained. Figure 17 shows the experimental set-up (left) and a typical fracture surface (right).

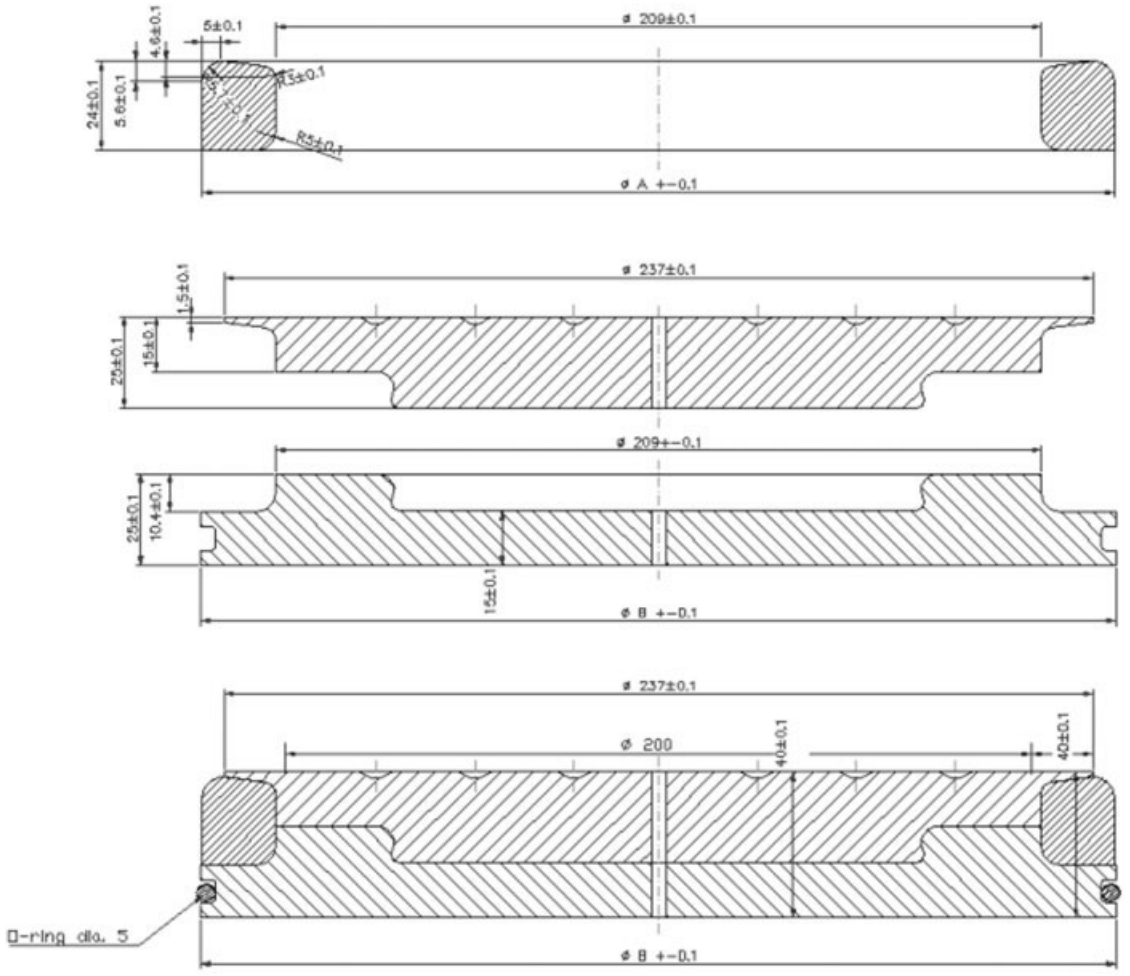

FIG. 15. Layout of the UHMWPE disc with a reinforcing carbon/epoxy ring (courtesy of SOLICO, solutions in composites).

 DOI 10.1002/pc

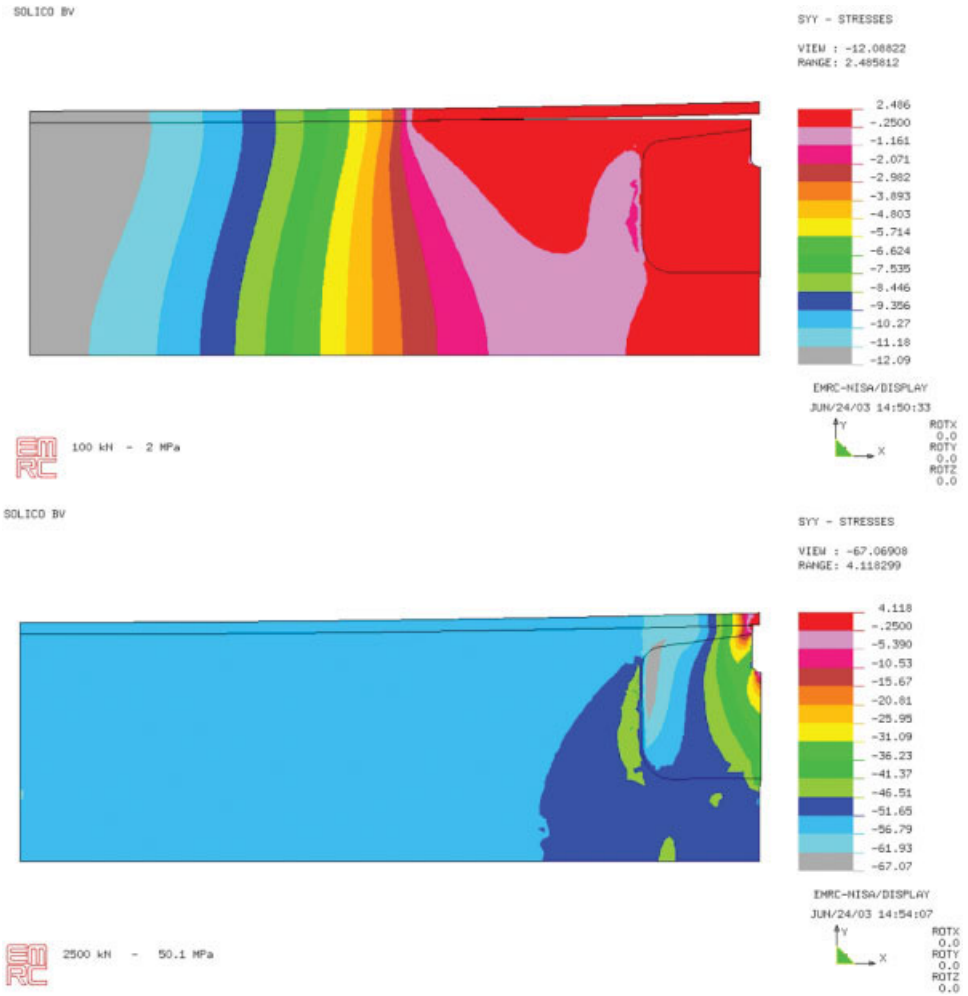

FIG. 16. Finite element simulation of the contact between the convex ball-joint surface and the composite material disc for a normal load of (i) 100 kN and (ii) 2,500 kN (courtesy of SOLICO, solutions in composites). [Color figure can be viewed in the online issue, which is available at www.interscience.wiley.com.]

Short-Beam Three-Point Bending Tests

Finally, short-beam three-point bending tests were applied, in agreement with the ASTM standard D2344/D2344M-00e1 Standard Test Method for Short-Beam Strength of Polymer Matrix Composite Materials and Their Laminates. The standard could only be satisfied partially, because the radial thickness of the rings was much larger than the allowed 6.5 mm in the ASTM standard. Because of the high machining costs for reducing the radial thickness, short segments of the ring were tested without any radial thickness reduction. Figure 18 shows the experimental set-up.

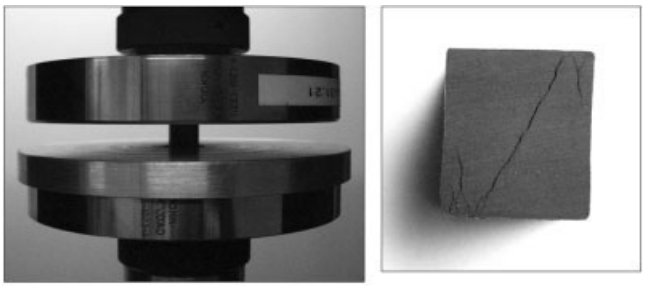

FIG. 17. Compression tests: experimental set-up (left) and failed specimen (right).

Typical failure patterns are shown in Fig. 19.

The short-beam three-point bending test appeared to be a very fast and reliable test method. The scatter of the results was very small, as illustrated by Fig. 20. This graph shows the recorded force-displacement graph for specimens cut from three different rings. The failure loads were 32.82, 33.19, and 33.55 kN.

CONCLUSIONS

In this article, two competing designs for an extremely high-loaded ball-joint were discussed. Both made use of fiber-reinforced composite materials, because all "traditional" materials appeared not suitable for the extreme load-

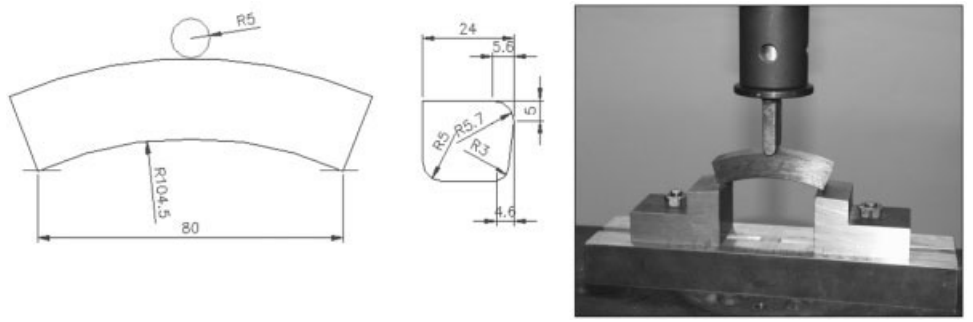

FIG. 18. Experimental set-up for the short-beam three-point bending test.

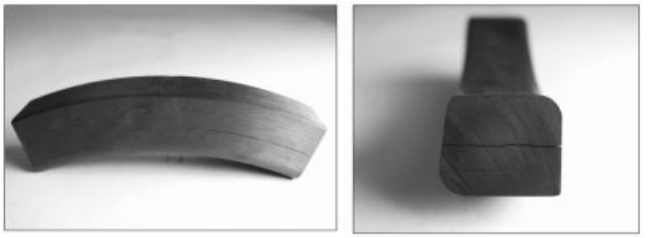

FIG. 19. Typical failure patterns of the short-beam specimens in three-point bending.

ing conditions. Testing methods were designed to assess the critical aspects of the design.

The second design met all specifications and was finally integrated in the ball-joints of the Maeslant storm surge barrier. Five hundred UHMWPE discs with reinforcing carbon/epoxy ring were placed in the holes of the pedestals, as shown in Fig. 21.

In September 2004, a successful test closing of the storm surge barrier was performed and inspections afterward revealed not any occurrence of damage.

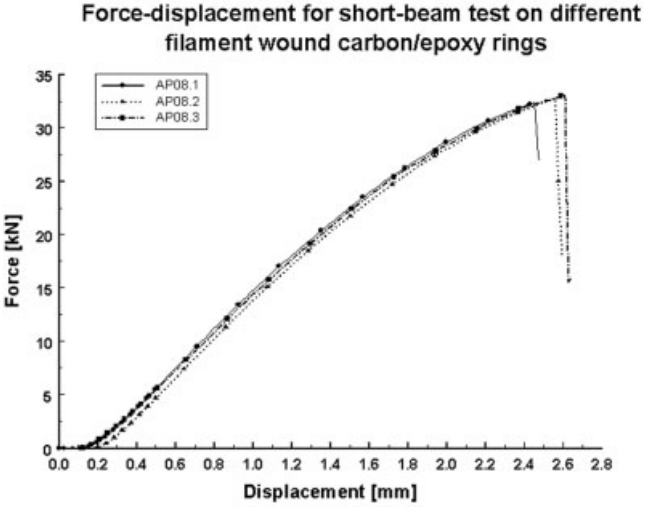

FIG. 20. Force-displacement path of the short-beam three-point bending test on specimens of three different rings.

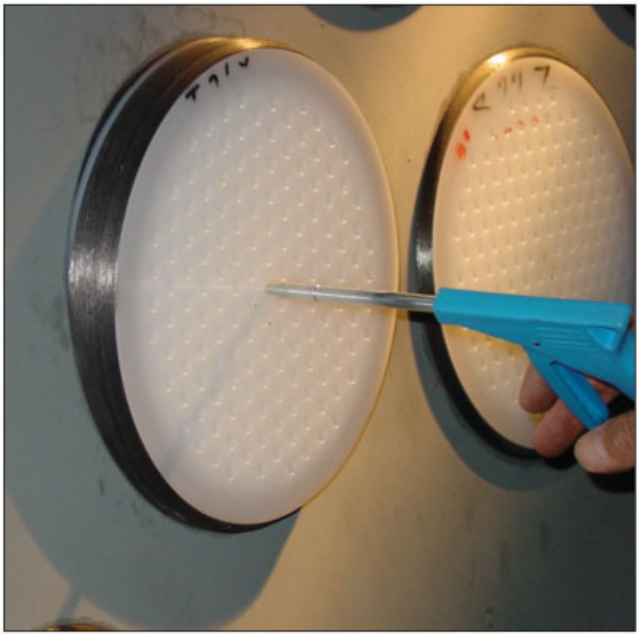

FIG. 21. Placement of the composite discs in the holes of the ball joint (courtesy of Rijkswaterstaat). [Color figure can be viewed in the online issue, which is available at www.interscience.wiley.com.]

ACKNOWLEDGMENTS

The authors express their gratitude to SOLICO BV, Solutions in Composites and the Ministry of Transport, Public Works, and Water Management in the Netherlands.

REFERENCES

1. Official English website of the Maeslant storm surge barrier in the Netherlands. Available at: www.keringhuis.nl/engels/keringhuis/index.html
2. H. Leendertz, L. Van Schepdael, W. Van Paepegem, P. Samyn, P. De Baets, and J. Degrieck, Anderung der gelenklagerkonstruktion des sturmflutsperrwerks bei Rotterdam. *Stalhbau*, **75**, 45–54 (2005).
3. D. Hull and T.W. Clyne, *An Introduction to Composite Materials*, Cambridge University Press, Cambridge, ISBN 0 521 28392 2 (1996).

 DOI 10.1002/pc